Available online at www.sciencedirect.com

SciVerse ScienceDirect

Ceramics International 39 (2013) 8467–8473

CERAMICS INTERNATIONAL

www.elsevier.com/locate/ceramint

Synthesis and characterization of morphologically tailored NiO–$Ce_{0.8}Gd_{0.2}O_{2-\delta}$ anode materials for solid oxide fuel cells: A micro-emulsion followed by solvothermal approach

Manas K. Rath[a], Byung-Hyun Choi[b], Ki-Tae Lee[a,c,*]

[a]Division of Advanced Materials Engineering, Chonbuk National University, Jeonbuk 561-756, Republic of Korea
[b]Energy Materials Center, Korea Institute of Ceramic Engineering and Technology, Seoul 153-801, Republic of Korea
[c]Hydrogen and Fuel Cell Research Center, Chonbuk National University, Jeonbuk 561-756, Republic of Korea

Received 26 February 2013; received in revised form 10 April 2013; accepted 10 April 2013
Available online 17 April 2013

Abstract

NiO–$Ce_{0.8}Gd_{0.2}O_{2-\delta}$ cermet anode powders with flake-shaped particles have been synthesized using a unique micro-emulsion-mediated solvothermal process. With an increase in the amount of urea used as a precipitation agent, the particles change from plate to flake shape in a morphological transition. Well-developed flake-shaped anode powders can be obtained from 24 h of solvothermal treatment. The polarization resistance at 800 °C in humidified H_2 and the activation energy of the anode synthesized with 1:4 salt to urea ratio and the solvothermal treatment duration of 24 h are 0.01 Ω cm^2 and 0.53 eV, respectively. In accordance with the polarization resistance results, a single cell with the MEST4 anode shows a high maximum-power density of 0.32 W cm^{-2}, at 800 °C with a humidified H_2 fuel.

Keywords: A. Micro-emulsion; C. Electrochemical performance; E. Solid oxide fuel cells; Solvothermal

1. Introduction

Solid oxide fuel cells (SOFC) are energy conversion devices that directly convert chemical fuel to electrical energy via an electrochemical reaction [1]. A thin electrolyte is separated by two electrodes, the anode and cathode. While a reduction of oxidant occurs at the cathode side, fuel oxidation occurs at the anode side. The electrochemical reaction occurs at the limited active area, called the triple phase boundary (TPB), where gas, electrolyte, and electrode meet [2,3]. Optimization of the TPB can provide excellent opportunities for performance improvement in SOFC [4,5]. In the case of anodes, the introduction of cermet, which is a composite of metal catalyst and electrolyte materials, is an effective approach for increasing the TPB length [6–8]. In this regard, Ni–yttria-stabilized zirconia (YSZ) is a state-of-the-art anode material; while Ni acts as a catalyst, YSZ provides the porous structure and also acts as an ionic conductor, transferring oxygen ions to the reaction site to finish the catalytic cycle. Recently, YSZ has been replaced with Gd-doped ceria (GDC), because GDC has higher ionic conductivity than YSZ and can offer catalytic activity, due to its mixed ionic–electronic conduction in a reduced atmosphere.

Many studies have explored the improvement of composite anode performance with respect to microstructure [9–12]. These focus on optimization related to the tailored microstructure of the anodes, which suggests TPB enlargement using nano-structured composite powders and various fabrication processes [13–19]. Suzuki et al. reported outstanding cell performance using Ni-cermet anodes with particle sizes of less than 100 nm [8].

In order to tailor the microstructure of the ceramic particles, it is essential to control the abnormal nucleation and growth of the crystals. It has been reported that the micro-emulsion process and reverse micelles are useful in controlling the growth of ceramic particles such as ZnO, TiO_2, and ZrO_2 [20–23]. The micro-emulsion method, however, has limitations when synthesizing

*Corresponding author at: Chonbuk Natioanl University, Division of Advanced Materials Engineering, 664-14 Deokjin-dong 1ga, Deokjin-gu, Jeonbuk 561-756 , Republic of Korea. Tel.: +82 63 270 2290; fax: +82 63 270 2386.
E-mail address: ktlee71@jbnu.ac.kr (K.-T. Lee).

0272-8842/$ - see front matter © 2013 Elsevier Ltd and Techna Group S.r.l. All rights reserved.
http://dx.doi.org/10.1016/j.ceramint.2013.04.029

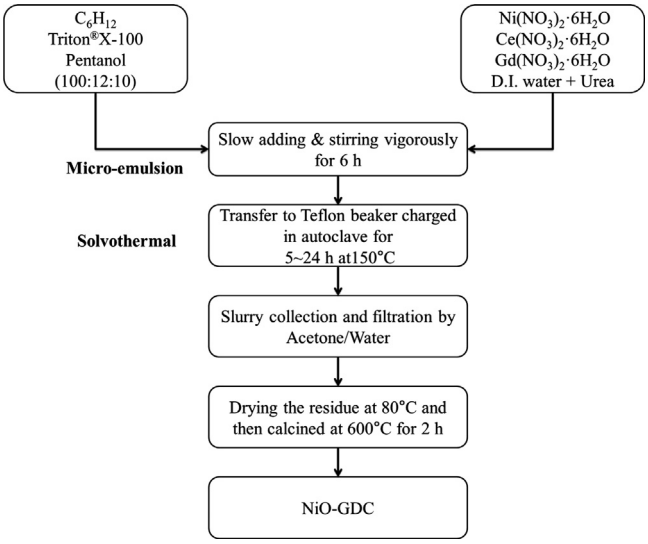

Fig. 1. Flow chart for the synthesis of morphologically-tailored NiO–GDC powders using a micro-emulsion-mediated solvothermal (MEST) process.

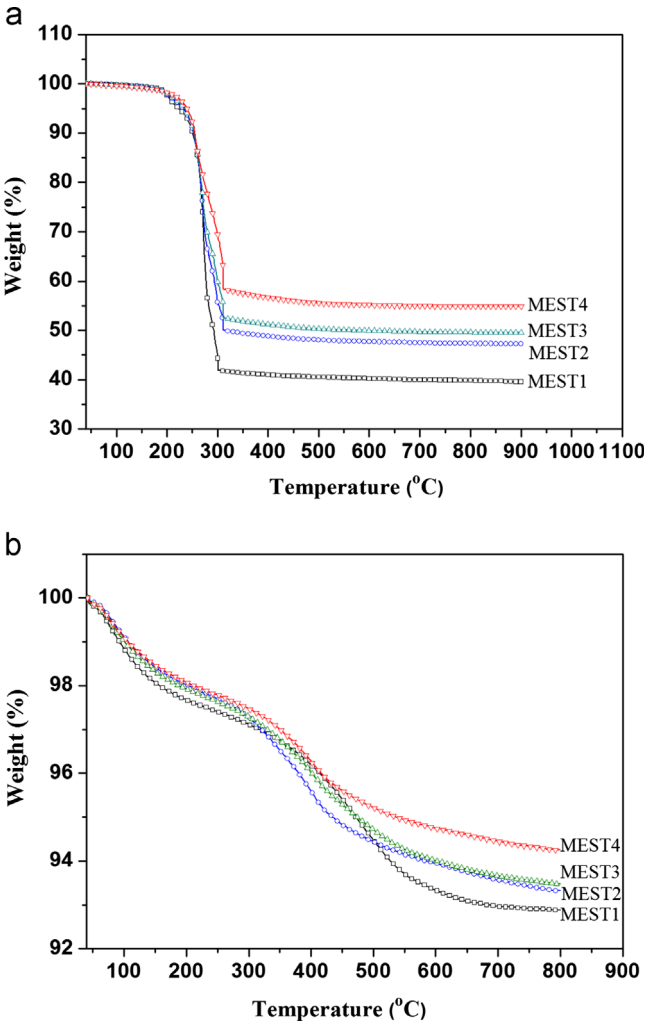

Fig. 2. TGA data of the NiO–GDC powders: (a) dry residue and (b) pre-calcined at 300 °C for 6 h.

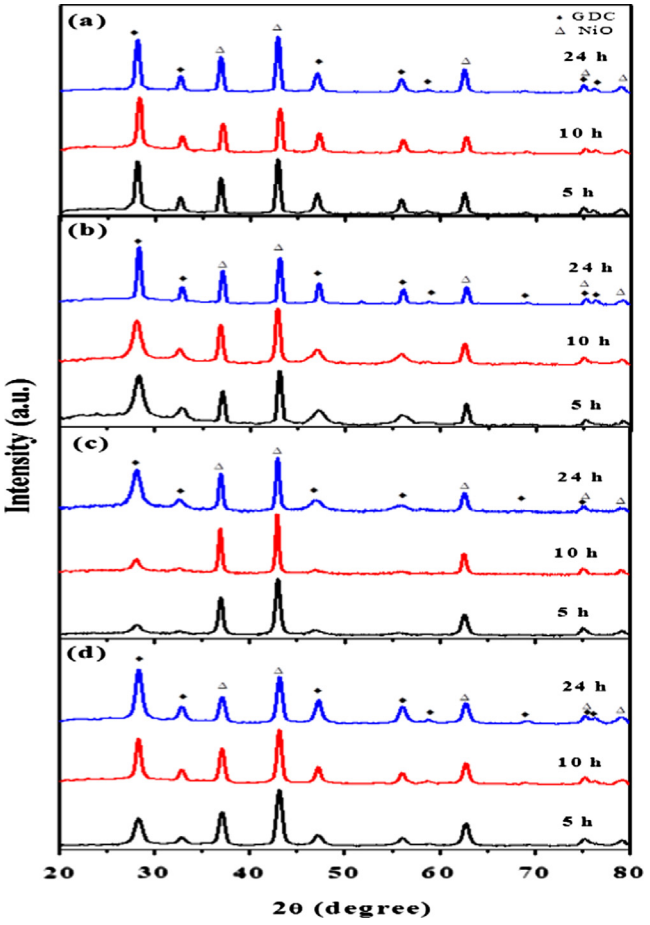

Fig. 3. XRD patterns of the as-synthesized NiO–GDC powders of (a) MEST1 (b) MEST2 (c) MEST3 and (d) MEST4 with respect to solvothermal treatment duration.

multiple component oxides or highly-ordered composite oxides. The solvothermal method has been used to synthesize various tailored-nanostructured inorganic materials such as whisker, ellipsoid, sphere, nano-fiber, and nano-rod [24–27]. We have adapted the solvothermal process as a post-treatment process for micro-emulsion in order to synthesize NiO–GDC composite powders with tailored morphology. This micro-emulsion-mediated solvothermal (MEST) synthesis method has advantages over the micro-emulsion method, in that it can decrease reaction temperature and improve the crystallinity of the products.

2. Experimental procedures

The morphologically-tailored NiO–GDC powders were synthesized using the novel micro-emulsion-mediated solvothermal (MEST) process. A micro-emulsion, which is a thermodynamically stable and isotropic liquid mixture of oil, water, and surfactant, was prepared, followed by a solvothermal treatment. The solvothermal method is similar to the hydrothermal process, which is prepared in an aqueous media, though the precursor solution for the solvothermal method is dissolved in organic solvents. The procedure for the synthesis of NiO–GDC powders using the micro-emulsion-mediated solvothermal method is illustrated in Fig. 1. The raw

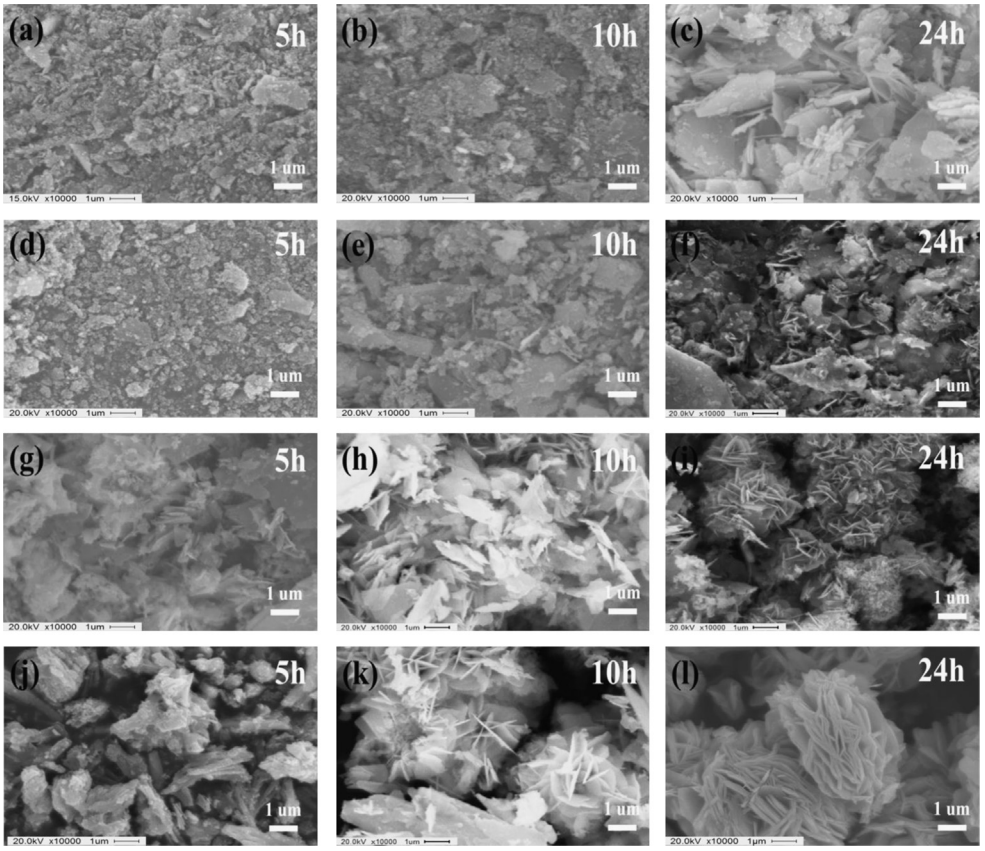

Fig. 4. SEM micrographs of the as-synthesized NiO–GDC powders of MEST1 (a–c), MEST2 (d–f), MEST3 (g–i) and MEST4 (j–l) with respect to solvothermal treatment duration.

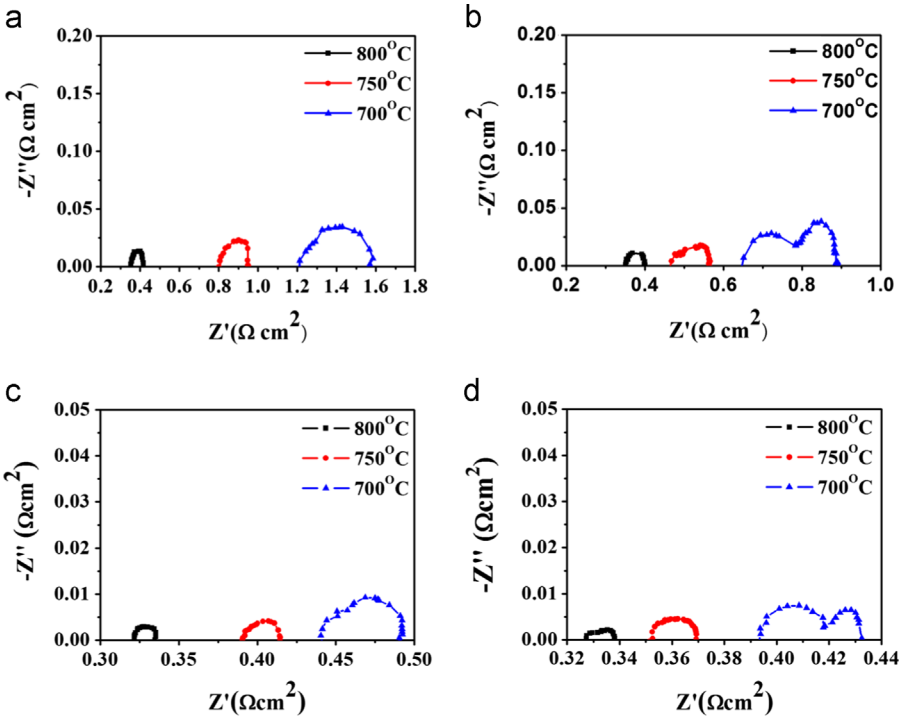

Fig. 5. Typical AC impedance spectra of the Ni–GDC anode of (a) MEST1, (b) MEST2 (c) MEST3 and (d) MEST4 at 800 °C in humidified H_2.

materials were $Ni(NO_3)_2 \cdot 6H_2O$ (Alfa Aesar, 98%), $Ce(NO_3)_3 \cdot 6H_2O$ (Aldrich, 99% metal basis), $Gd(NO_3)_3 \cdot xH_2O$ ($x=6$, Alfa Aesar, 99.9%, REO), cyclohexane (C_6H_{12}, Alfa Aesar, 99+%), Triton®X-100 ($C_{14}H_{22}O(C_2H_4O)_n$, Alfa-Aesar), 1-pentanol ($C_5H_{12}O$, Alfa Aesar, 98+%), acetone (Samchun Chemicals, 99.5%), and urea (Alfa-Aesar, 98+%) as a precipitation agent. De-ionized water was used for the aqueous phase. Four types of NiO–GDC powders were prepared using the micro-emulsion-mediated solvothermal method with various molar concentration ratios of nitrate salt (S) to urea (U), S:U = 1:1, 1:2, 1:3, and 1:4, in the aqueous phase, and named MEST1, MEST2, MEST3, and MEST4, respectively. In order to investigate the effect of solvothermal treatment time on the morphology of NiO–GDC, solvothermal treatment was carried out at dwelling times of 5 h, 10 h, and 24 h for each sample. Finally, the gathered powders were calcined at 600 °C for 2 h in air.

The as-synthesized, morphologically tailored NiO–GDC anode powders were characterized by X-ray diffraction (XRD) using Cu-Kα radiation. The morphology of the powders and the microstructural characterizations of the sintered samples were investigated with scanning electron microscopy (SEM, SN-3000 Hitachi, Japan). The specific surface area of each powder was measured by BET (Brunauer, Emmett, Teller) analysis (ASAP2010 physisorption analyzer, Micrometrics, USA). Thermogravimetric analysis (TGA, TA Q600, TA instruments, USA) was carried out in order to verify the micro-emulsion-mediated solvothermal process. TGA was performed in air with a temperature range of 30–800 °C, and a heating rate of 10 °C min^{-1}.

The catalytic activity and electrochemical performance of the synthesized Ni–GDC anode were evaluated with AC impedance analysis and a single cell test, respectively, using an electrolyte-supported single cell. Coin-shaped GDC electrolyte pellets with a 25 cm diameter and 0.5 mm thickness were fabricated using commercial GDC powder (CGO90/10 UHSA, Grand C&M Co. Ltd.), and sintered at 1450 °C for 4 h. $Ba_{0.5}Sr_{0.5}Co_{0.8}Fe_{0.2}O_{3-\delta}$–$Ce_{0.8}Gd_{0.2}O_{2-\delta}$ (50:50 wt%/wt%) powder, synthesized with the combustion method, was used as a cathode [28]. Each electrode layer with a geometrical area of 0.49 cm^2 was fabricated by screen-printing on both sides of the GDC pellet. Both anode and cathode pastes were made by mixing the powder and binder (Heraeus V006) at a ratio of 70:30 wt%. Each screen-printed anode and cathode layer was fired at 1250 °C and 1050 °C, respectively, for 2 h. Single-cell AC impedance analysis was performed using a universal potentiostat with a frequency response analyzer (Bio-logic Science Instruments), and a three-electrode configuration under humidified H_2 at 700 °C, 750 °C, and 800 °C. The applied frequency was in the range from 1 mHz to 1 MHz, with a voltage amplitude of 10 mV. *I–V* measurements of single cells were carried out using a fuel cell test station (SMART2, WonATech Co. Ltd., Korea) at 700 °C, 750 °C, and 800 °C. Humidified H_2 (~3% H_2O at 30 °C) and dry air were supplied as fuel and oxidant, respectively, at a rate of 100 cm^3 min^{-1}. NiO in the anode was reduced to Ni in humidified H_2 before the AC impedance analysis and single cell test.

3. Results and discussion

TGA plots of NiO–GDC powder synthesized by the micro-emulsion-mediated solvothermal process are shown in Fig. 2. At 200 °C, a significant weight loss occurred in the dry residue, which became saturated at approximately 300 °C. The total weight losses in the temperature range of 200–300 °C for MEST1, MEST2, MEST3, and MEST4 were 60.5%, 52.8%, 50.4%, and 42.2%, respectively. The weight losses in the NiO–GDC residue were due to the presence of water and organic solvents. After further heating to 900 °C, a weight loss of approximately 4% was recorded. These weight losses correspond to the conversion of hydroxide, or other pre-phase NiO–GDC, to the final oxide phase. The total weight loss in all NiO–GDC residues was approximately 56 ± 5 wt%, which is significantly larger than the theoretical weight loss during decomposition of the $Ni(OH)_2$ to NiO (17.8%), and of the $Ce(OH)_4$ to CeO_2 (17.3%) [29,30]. This difference is due to the presence of a large amount of organic residue in the micro-emulsion. The dry residues were pre-calcined at 300 °C in order to confirm the decomposition process and clearly determine the calcination temperature. As shown in Fig. 2 (b), two significant weight losses are distinctly visible in the TGA plots. The first occurs from room temperature to approximately 300 °C, and is due to the loss of crystal water as well as some organic components. The recorded weight losses are 2.4%, 2.9%, 2%, and 1.9% for MEST1, MEST2, MEST3, and MEST4, respectively. The second weight loss occurred from 300 °C to 600 °C; the weight losses measured in this temperature range were 4.3%, 4%, 3.2%, and 3.3% for MEST1, MEST2, MEST3, and MEST4, respectively. This weight loss corresponds to the decomposition of hydroxide to oxide phases. Additionally, a certain amount of CO_2 and H_2O were produced as byproducts during the formation of NiOH and $Gd/Ce(OH)_4$, due to the decomposition of urea to ammonia by hydrolysis [31,32]. The TGA data also shows that in order to obtain pure NiO–GDC powders, a calcination temperature of over 600 °C should be used.

XRD patterns of the as-synthesized NiO–GDC powders calcined at 600°C for the appropriate solvothermal treatment durations are given in Fig. 3. Peaks for all samples are well matched with cubic NiO (Fm3m, JCPDF #47-1049) and cubic $Ce_{0.8}Gd_{0.2}O_{2-\delta}$ (Fm3m, JCPDF #34-0394), and no secondary phase or impurity was detected. Using Scherrer's formula, the calculated mean crystallite sizes of NiO and GDC were found to be 22 ± 2 nm and 20 ± 2 nm, respectively, irrespective of the solvothermal treatment duration.

Although no significant variation in crystallite size was observed, the overall morphology of the as-synthesized NiO–GDC powders was found to strongly depend on both the salt to urea ratio and the solvothermal treatment duration, as shown in Fig. 4. Unlike the calculated mean crystallite size results, the particle size of the as-synthesized NiO–GDC powders increased with an increase in urea content. As the solvothermal treatment time increased, a morphology transition occurred. Interestingly, while particles in the NiO–GDC powders synthesized with a low urea concentration (MEST1 and MEST2) and at a solvothermal treatment time of 24 h were plate shaped, those synthesized with a high urea concentration (MEST3 and MEST4) formed flake-like

microspheres, with flakes resembling flower petals. The growth process of the unique flake-like structure may be associated with the urea, which has a planar-crystal structure and two $-NH_2$ groups joined by a carbonyl (C═O) functional group [33]. The oxygen center is engaged in two N–H–O hydrogen bonds [32]. The structure of urea is quite open and flat, and the H-bonded networks and ribbons form tunnels with a square cross-section. Considering the structure of urea, it is expected that during the solvothermal treatment the Ni, Gd, and Ce precursors are precipitated and bound with the planner H-bonded network of the urea. The formation of flakes therefore begins with a small seeding, ultimately forming large flakes or flower-like morphology. One can easily expect that the flake-like microsphere anode powder would have a large specific surface area. The BET surface areas of the MEST1, MEST2, MEST3, and MEST4 anode powders were 10.6 $m^2 g^{-1}$, 12.2 $m^2 g^{-1}$, 28.5 $m^2 g^{-1}$, and 32.6 $m^2 g^{-1}$, respectively. Considering the catalytic reaction on the anode surface, one may expect the MEST4 anode with the largest surface area to exhibit the best electrochemical performance.

The AC impedance spectra of Ni–GDC anodes in humidified H_2 are shown in Fig. 5. While the left intercept with the impedance arc on the Z′-axis at high frequencies indicates the ohmic resistance, R_o, the right intercept on the Z′-axis at low frequencies corresponds to the total resistance, R_{tot}. The polarization resistance, R_p, is the overall size of the arcs (R_{tot}–R_o). The calculated R_p values at 700 °C, 750 °C, and 800 °C are listed in Table 1. The MEST4 anode showed lower R_p value at a given temperature in H_2. With respect to the reaction sites, it can be expected that the MEST4 anode with the well-developed flake structure, as shown in Fig. 4, would show better electrochemical performance than the other anodes. The temperature dependences of the ohmic (R_o) and polarization (R_p) resistances are shown in Fig. 6, and the calculated activation energy, E_a, values are listed in Table 1. The activation energy of the Ni–GDC anode synthesized by the micro-emulsion-mediated solvothermal process is relatively lower than that of other Ni–ceria-based anodes investigated earlier (0.9–1.45 eV) [34–36].

Fig. 7 shows the SEM micrographs of the Ni–GDC anodes after the electrochemical performance test. It is well known that the initial morphology of a powder strongly affects the final structure of the sintered body. Although the anodes do not hold the flake shape due to high-temperature sintering, they still have a small grain size, less than 1 μm, appropriate area contact between grains, and good adhesion between the anode and electrolyte.

I–V curves and power densities for the Ni–GDC anode synthesized by the micro-emulsion-mediated solvothermal process are shown in Fig. 8. The maximum power densities of a single cell with the MEST1, the MEST2, the MEST3, and the MEST4 anode at 800 °C in humidified H_2 were 0.21 W cm^{-2}, 0.29 W cm^{-2}, 0.30 W cm^{-2}, and 0.32 W cm^{-2}, respectively. Although there was no significant difference in the single cell performance, it is consistent with the trend observed in the AC impedance data.

4. Conclusions

NiO–GDC cermet anode powders with flake-shaped particles were successfully synthesized using a unique micro-emulsion-mediated solvothermal process. Control of the morphological transition was made possible by altering both the ratio of salt to urea and the solvothermal treatment duration. The particle morphology changed from plate to flake shape with an increase in urea concentration, and a solvothermal treatment time of over 24 h was required to obtain well-developed flake-like microsphere anode powders. The initial flake-like Ni–GDC powders tended to form a highly-porous network structure with small grain size, even after the final sintering stage, which led to an improvement in electrochemical performance.

Table 1
Polarization resistance and activation energy of the Ni–GDC anodes at various operating temperatures in humidified H_2.

Anode material	Polarization resistance (Ω cm^2)			Activation energy (eV)
	700 °C	750 °C	800 °C	
MEST1	0.355	0.152	0.064	0.72
MEST2	0.244	0.100	0.047	0.67
MEST3	0.050	0.024	0.013	0.56
MEST4	0.039	0.017	0.011	0.53

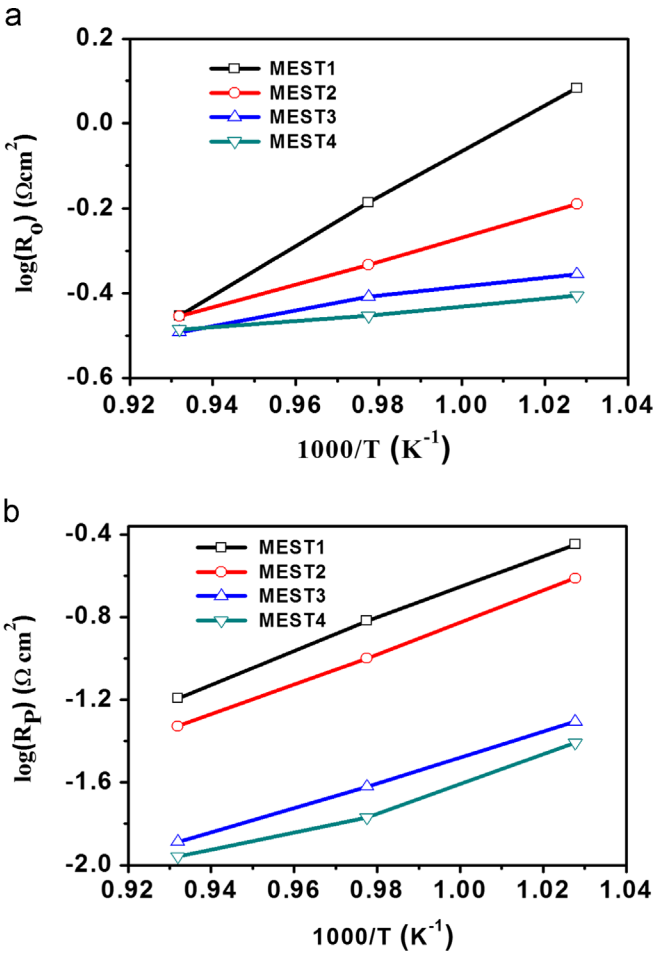

Fig. 6. Temperature dependence of (a) ohmic (R_o) and (b) polarization (R_p) resistances of Ni–GDC anodes in humidified H_2.

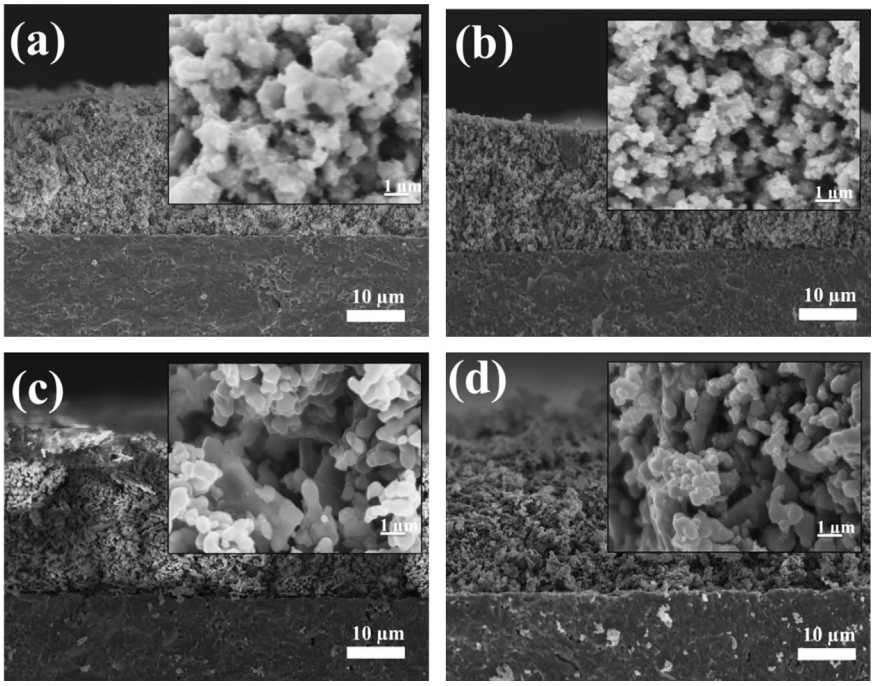

Fig. 7. SEM micrographs of the NiO–GDC anodes of (a) MEST1, (b) MEST2 (c) MEST3 and (d) MEST4 fired at 1250 °C for 2 h. The inset shows an enlarged micrograph of the anode region.

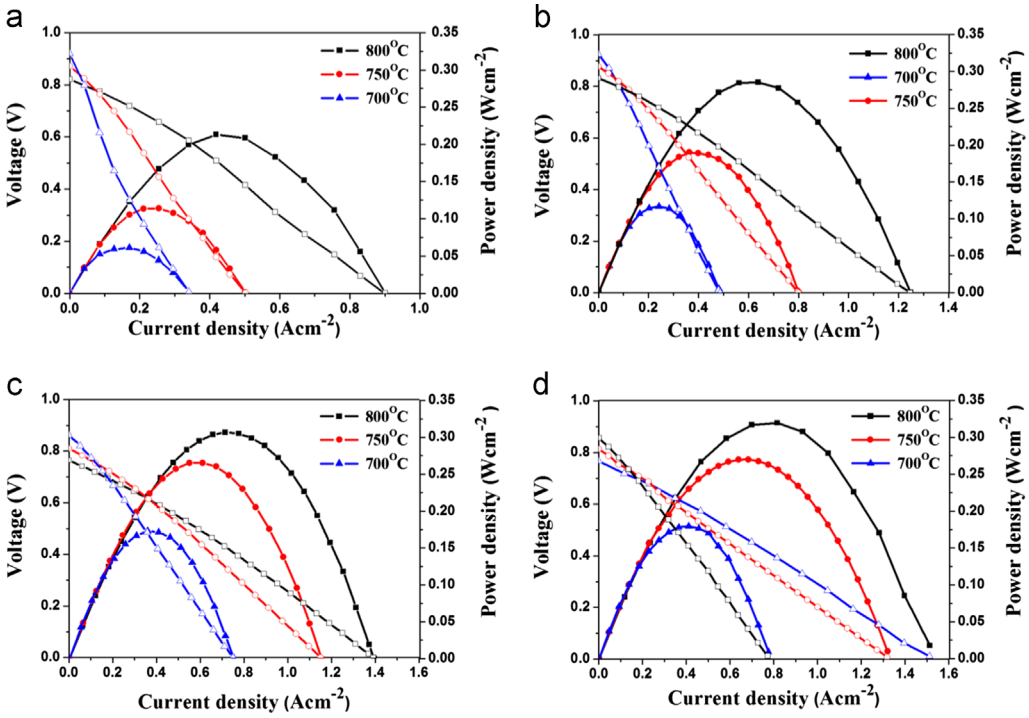

Fig. 8. Comparison of the *I–V* curves (open symbols) and power densities (closed symbols) of Ni–GDC anodes: (a) MEST1, (b) MEST2 (c) MEST3 and (d) MEST4 anodes.

Acknowledgments

This work was supported by a New & Renewable Energy grant from the Korea Institute of Energy Technology Evaluation and Planning (KETEP) funded by the Korean Ministry of Knowledge Economy (2010T100100622). This work was also supported by the Human Resources Development of the Korea Institute of Energy Technology Evaluation and Planning (KETEP) grant funded by the Korea Government Ministry of Knowledge Economy (No. 20114030200060).

References

[1] N.Q. Minh, Ceramic fuel cells, Journal of the American Ceramic Society 76 (1993) 563–588.

[2] S.C. Singhal, Advances in solid oxide fuel cell technology, Solid State Ionics 135 (2000) 305–313.

[3] J. Maier, Ionic conduction in space charge regions, Progress in Solid State Chemistry 23 (1995) 171–263.

[4] R.J. Kee, H. Zhu, D.G. Goodwin, Solid-oxide fuel cells with hydrocarbon fuels, Proceedings of the Combustion Institute 30 (2005) 2379–2404.

[5] S.D. Kim, H. Moon, S.H. Hyun, J. Moon, J. Kim, H.W. Lee, Nano-composite materials for high-performance and durability of solid oxide fuel cells, Journal of Power Sources 163 (2006) 392–397.

[6] B.C.H. Steele, Material science and engineering: the enabling technology for the commercialisation of fuel cell systems, Journal of Materials Science 36 (2001) 1053–1068.

[7] J. Mizusaki, H. Tagawa, K. Tsuneyoshi, A. Sawata, Reaction kinetics and microstructure of the solid oxide fuel cells air electrode $La_{0.6}Ca_{0.4}MnO_3$/YSZ, Journal of the Electrochemical Society 138 (1991) 1867–1873.

[8] T. Suzuki, Z. Hasan, Y. Funahashi, T. Yamaguchi, Y. Fujishiro, M. Awano, Impact of anode microstructure on solid oxide fuel cells, Science 325 (2009) 852–855.

[9] J. Deseure, Y. Bultel, L. Dessemond, E. Siebert, Theoretical optimisation of a SOFC composite cathode, Electrochimica Acta 50 (2005) 2037–2046.

[10] C.W. Tanner, K.Z. Fung, A.V. Virkar, The effect of porous composite electrode structure on solid oxide fuel cell performance: I. Theoretical analysis, Journal of the Electrochemical Society 144 (1997) 21–30.

[11] S.H. Chan, Z.T. Xia, Anode micro-model of solid oxide fuel cell, Journal of the Electrochemical Society 148 (2001) A388–A394.

[12] R. O'Hayre, D.M. Barnett, F.B. Prinz, The triple phase boundary: a mathematical model and experimental investigations for fuel cells, Journal of the Electrochemical Society 152 (2005) A439–A444.

[13] T. Fukui, S. Ohara, M. Naito, K. Nogi, Morphology control of the electrode for solid oxide fuel cells by using nanoparticles, Journal of Nanoparticle Research 3 (2001) 171–174.

[14] M. Mamak, G.S. Metraux, S. Petrov, N. Coombs, G.A. Ozin, M.A. Green, Lanthanum strontium manganite/yttria-stabilized zirconia nanocomposites derived from a surfactant assisted, co-assembled mesoporous phase, Journal of the American Chemical Society 125 (2003) 5161–5175.

[15] D.S. Lee, J.H. Lee, J. Kim, H.W. Lee, H.S. Song, Tuning of the microstructure and electrical properties of SOFC anode via compaction pressure control during forming, Solid State Ionics 166 (2004) 13–17.

[16] V. Esposito, D.Z. de Florio, F.C. Fonseca, E.N.S. Muccillo, R. Muccillo, E. Traversa, Electrical properties of YSZ/NiO composites prepared by a liquid mixture technique, Journal of the European Ceramic Society 25 (2005) 2637–2641.

[17] C. Lu, T.Z. Sholklapper, C.P. Jacobson, S.J. Visco, L.C. De Jonghe, LSM–YSZ cathodes with reaction-infiltrated nanoparticles, Journal of the Electrochemical Society 153 (2006) A1115–A1119.

[18] S.P. Jiang, S. Zhang, Y.D. Zhen, A.P. Koh, Performance of GDC-impregnated Ni anodes of SOFCs, Electrochemical and Solid-State Letters 7 (2004) A282–A285.

[19] W. Zhu, D. Ding, C. Xia, Enhancement in three-phase boundary of SOFC electrodes by an ion impregnation method: a modeling comparison, Electrochemical and Solid-State Letters 11 (2008) B83–B86.

[20] A.K. Ganguli, T. Ahmad, S. Vaidya, J. Ahmed, Microemulsion route to the synthesis of nanoparticles, Pure and Applied Chemistry 80 (2008) 2451–2477.

[21] M.P. Pileni, Reverse micelles used as templates: a new understanding in nanocrystal growth, Journal of Experimental Nanoscience 1 (2006) 13–27.

[22] M.A. Lo´pez-Quintela, Synthesis of nanomaterials in microemulsions: formation mechanisms and growth control, Current Opinion in Colloid and Interface Science 8 (2003) 137–144.

[23] B.K. Paul, S.P. Moulik, Uses and applications of microemulsions, Current Science 80 (2001) 990–1001.

[24] M.H. Cao, X. Wu, X. He, C. Hu, Microemulsion-mediated solvothermal synthesis of $SrCO_3$ nanostructures, Langmuir 21 (2005) 6093–6096.

[25] M.H. Cao, C.W. Hu, E.B. Wang, The first fluoride one-dimensional nanostructures: microemulsion-mediated hydrothermal synthesis of BaF_2 whiskers, Journal of the American Chemical Society 125 (2003) 11196–11197.

[26] M.H. Cao, C.X. Guo, Y.J. Qi, C.W. Hu., E.B. Wang, Preparation of ultrahigh-aspect-ratio hydroxyapatite nanofibers in reverse micelles under hydrothermal conditions, Langmuir 20 (2004) 4784–4786.

[27] M.H. Cao, Y.H. Wang, Y.J. Qi, C.X. Guo, C.W. Hu, Synthesis and characterization of MgF_2 and $KMgF_3$ nanorods, Journal of Solid State Chemistry 177 (2004) 2205–2209.

[28] M.K. Rath, B.H. Choi, K.T. Lee, Properties and electrochemical performance of $La_{0.75}Sr_{0.25}Cr_{0.5}Mn_{0.5}O_{3-\delta}$–$La_{0.2}Ce_{0.8}O_{2-\delta}$ composite anodes for solid oxide fuel cells, Journal of Power Sources 213 (2012) 55–62.

[29] A.I.Y. Tok, F.Y.C. Boey, Z. Dong, X.L. Sun, Hydrothermal synthesis of CeO_2 nano-particles, Journal of Materials Processing Technology 190 (2007) 217–222.

[30] Y.P. Fu, C.H. Lin, Microwave-induced combustion synthesis of Ni–Zn ferrite powder and its characterization, Journal of Magnetism and Magnetic Materials 251 (2002) 74–79.

[31] R.K. Sahu, A.K. Ray, S.K. Das, A.J. Kailath, L.C. Pathak, Microwave-assisted combustion synthesis of Ni powder using urea, Journal of Materials Research 21 (2006) 1664–1673.

[32] P.D. Godfrey, R.D. Brown, A.N. Hunter, The shape of urea, Journal of Molecular Structure 413–414 (1997) 405–414.

[33] S. Swaminathan, B.M. Craven, R.K. McMullan, The crystal structure and molecular thermal motion of urea at 12, 60, and 123 K from neutron diffraction, Acta Crystallographica B40 (1984) 300–306.

[34] S. Primdahl, Y.L. Liu, Ni catalyst for hydrogen conversion in gadolinia-doped ceria anodes for solid oxide fuel cells, Journal of the Electrochemical Society 149 (2002) A1466–A1472.

[35] U.P. Muecke, K. Akiba, A. Infortuna, T. Salkus, N.V. Stus, L.J. Gauckler, Electrochemical performance of nanocrystalline nickel/gadolinia-doped ceria thin film anodes for solid oxide fuel cells, Solid State Ionics 178 (2008) 1762–1768.

[36] S. Wang, M. Ando, T. Ishihara, Y. Takita, High performance Ni–$Sm_{0.15}Ce_{0.85}O_{2-\delta}$ cermet anodes for intermediate temperature solid oxide fuel cells using $LaGaO_3$ based oxide electrolytes, Solid State Ionics 174 (2004) 49–55.